

Issues and Algorithms for Tracking Multiple Sources with a Network of Sensors

Richard J. Kozick

Bucknell University
Department of Electrical Engineering
Lewisburg, PA 17837

Brian M. Sadler

Army Research Laboratory
AMSRL-CI-CN
2800 Powder Mill Road
Adelphi, MD 20783

Abstract

This paper presents issues and algorithms for the problem of multiple source tracking with a network of aeroacoustic sensors. We study fusion of data from sensors that are widely separated, and we give particular attention to the important issues of limited communication bandwidth between sensor nodes, effects of source motion, coherence loss between signals measured at different sensors, signal bandwidth, and noise. We compare the tracking performance of various schemes, including joint (coherent) processing of all sensor data, as well as data-reduction schemes that employ distributed computation and reduced communication bandwidth with a fusion center. Our analysis provides a quantification of the potential gain in source tracking accuracy that is achievable with greater communication bandwidth and joint processing of sensor data. We show that the potential gain in accuracy depends critically on the scenario, as determined by the source motion parameters, signal coherence between sensors, bandwidth of the source signals, and noise level. For scenarios that admit increased accuracy with joint processing, we present a bandwidth-efficient algorithm that involves beamforming at small-aperture sensor arrays combined with time-delay estimation between widely-spaced sensor arrays.

1 INTRODUCTION

We are concerned with tracking moving sources using a network of aeroacoustic sensors. We assume that the sensors are placed in an “array of arrays” configuration containing several small-aperture arrays distributed over a wide area. Each array contains local processing capability and a communication link with a fusion center. A standard approach for estimating the source locations involves bearing estimation at the individual arrays, communication of the bearings to the fusion center, and processing of the bearing estimates at the fusion center with a tracking algorithm (e.g., see [1, 2, 3, 4, 5]). This approach is characterized by low communication bandwidth and low complexity, but the localization accuracy may be inferior to the optimal solution in which the fusion center jointly processes all of the sensor data. The optimal solution requires high communication bandwidth and high processing complexity. The amount of improvement in localization accuracy that is enabled by greater communication bandwidth and processing complexity is dependent on the scenario, which we characterize in terms of the source motion parameters, the power spectra (and bandwidth) of the signals and noise in the sensor data, the coherence between the source signals received at widely separated sensors, and the observation time (amount of data). We present a framework in this paper to identify scenarios that have the potential for improved localization

Report Documentation Page

Report Date 25FEB2002	Report Type N/A	Dates Covered (from... to) -
Title and Subtitle Issues and Algorithms for Tracking Multiple Sources with a Network of Sensors		Contract Number
		Grant Number
		Program Element Number
Author(s)		Project Number
		Task Number
		Work Unit Number
Performing Organization Name(s) and Address(es) Bucknell University Department of Electrical Engineering Lewisburg, PA 17837		Performing Organization Report Number
Sponsoring/Monitoring Agency Name(s) and Address(es) Department of the Army, CECOM RDEC Night Vision & Electronic Sensors Directorate AMSEL-RD-NV-D 10221 Burbeck Road Ft. Belvoir, VA 22060-5806		Sponsor/Monitor's Acronym(s)
		Sponsor/Monitor's Report Number(s)
Distribution/Availability Statement Approved for public release, distribution unlimited		
Supplementary Notes Papers from 2001 Meeting of the MSS Specialty Group on Battlefield Acoustic and Seismic Sensing, Magnetic and Electric Field Sensors, Volume 1: Special Session held 23 Oct 2001. See also ADM001434 for whole conference on cd-rom.		
Abstract		
Subject Terms		
Report Classification unclassified	Classification of this page unclassified	
Classification of Abstract unclassified	Limitation of Abstract UU	
Number of Pages 19		

accuracy relative to the standard bearings-only tracking method. We propose an algorithm that is bandwidth-efficient and nearly optimal that uses beamforming at small-aperture sensor arrays and time-delay estimation between widely-separated sensors.

The sensor signals are modeled as Gaussian random processes, which allows deterministic as well as random propagation effects to be included. Our previous work [6, 7] considered a single source with fixed position (no motion). We extend the analysis in this paper to moving sources that follow a parametric motion model.

This paper is organized as follows. The sensor data model is presented in Section 2 for the case of a non-moving source. Results on time-delay estimation with partially-coherent signals are presented in Section 3, which summarizes and extends the development in [7]. The sensor data model is extended to moving sources in Section 4. An algorithm is presented in Section 5, an example with measured aeroacoustic data is included in Section 6, and concluding remarks are given in Section 7.

2 DATA MODEL FOR A NON-MOVING SOURCE

A model is formulated in this section for the discrete-time signals received by the sensors in distributed arrays. To begin, we consider a single non-moving source that is located at coordinates (x_s, y_s) in the (x, y) plane. Then H arrays are distributed in the same plane, as illustrated in Figure 1. Each array $h \in \{1, \dots, H\}$ contains N_h sensors, and has a reference sensor located at coordinates (x_h, y_h) . The location of sensor $n \in \{1, \dots, N_h\}$ is at $(x_h + \Delta x_{hn}, y_h + \Delta y_{hn})$, where $(\Delta x_{hn}, \Delta y_{hn})$ is the relative location with respect to the reference sensor. If c is the speed of propagation, then the propagation time from the source to the reference sensor on array h is

$$\tau_h = \frac{d_h}{c} = \frac{1}{c} \left[(x_s - x_h)^2 + (y_s - y_h)^2 \right]^{1/2}, \quad (1)$$

where d_h is the distance from the source to array h . We model the wavefronts over individual array apertures as perfectly coherent plane waves. Then in the far-field approximation, the propagation time from the source to sensor n on array h is expressed by $\tau_h + \tau_{hn}$, where

$$\tau_{hn} \approx -\frac{1}{c} \left[\frac{x_s - x_h}{d_h} \Delta x_{hn} + \frac{y_s - y_h}{d_h} \Delta y_{hn} \right] = -\frac{1}{c} [(\cos \phi_h) \Delta x_{hn} + (\sin \phi_h) \Delta y_{hn}] \quad (2)$$

is the propagation time from the reference sensor on array h to sensor n on array h , and ϕ_h is the bearing of the source with respect to array h . Note that while the far-field approximation (2) is reasonable over individual array apertures, the wavefront curvature that is inherent in (1) must be retained in order to model wide separations between arrays.

The time signal received at sensor n on array h due to the source will be represented as $s_h(t - \tau_h - \tau_{hn})$, where the vector of signals $\mathbf{s}(t) = [s_1(t), \dots, s_H(t)]^T$ received at the H arrays are modeled as real-valued, continuous-time, zero-mean, jointly wide-sense stationary, Gaussian random processes with $-\infty < t < \infty$. These processes are fully specified by the $H \times H$ cross-correlation function matrix

$$\mathbf{R}_s(\tau) = E\{\mathbf{s}(t + \tau) \mathbf{s}(t)^T\}, \quad (3)$$

where E denotes expectation, superscript T denotes transpose, and we will later use the notation superscript $*$ and superscript H to denote complex conjugate and conjugate transpose, respectively. The (g, h) element in (3) is the cross-correlation function

$$r_{s,gh}(\tau) = E\{s_g(t + \tau) s_h(t)\} \quad (4)$$

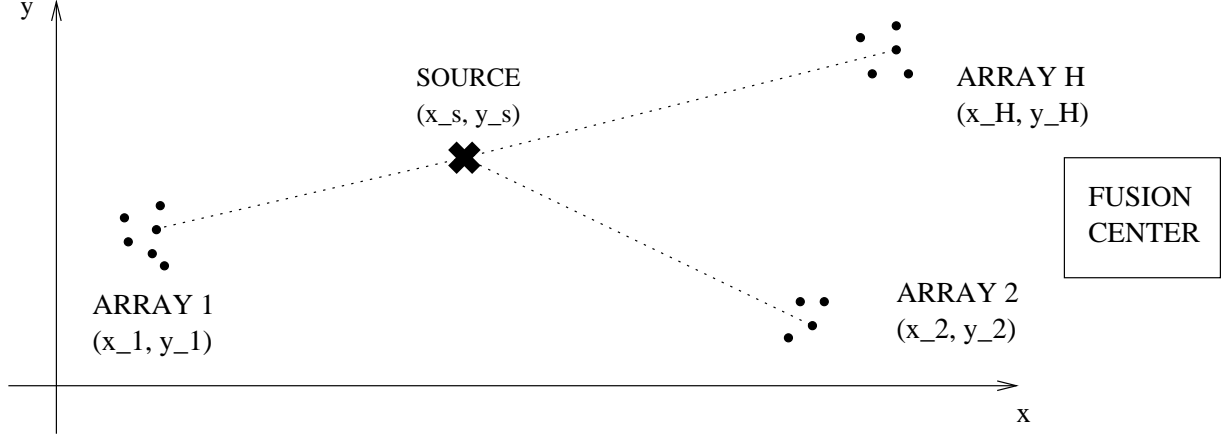


Figure 1: Geometry of non-moving source location and H distributed sensor arrays. A communication link is available between each array and the fusion center.

between the signals received at arrays g and h . The correlation functions (3) and (4) are equivalently characterized by their Fourier transforms, which are the cross-spectral density functions

$$G_{s,gh}(\omega) = \mathcal{F}\{r_{s,gh}(\tau)\} = \int_{-\infty}^{\infty} r_{s,gh}(\tau) \exp(-j\omega\tau) d\tau \quad (5)$$

and the associated cross-spectral density matrix

$$\mathbf{G}_s(\omega) = \mathcal{F}\{\mathbf{R}_s(\tau)\}. \quad (6)$$

The diagonal elements $G_{s,hh}(\omega)$ of (6) are the power spectral density (PSD) functions of the signals $s_h(t)$, and hence they describe the distribution of average signal power with frequency. The model allows the PSD to vary from one array to another to reflect propagation differences and source aspect angle differences.

The off-diagonal elements of (6), $G_{s,gh}(\omega)$, are the cross-spectral density (CSD) functions for the signals $s_g(t)$ and $s_h(t)$ received at distinct arrays $g \neq h$. In general, the CSD functions have the form

$$G_{s,gh}(\omega) = \gamma_{s,gh}(\omega) [G_{s,gg}(\omega)G_{s,hh}(\omega)]^{1/2}, \quad (7)$$

where $\gamma_{s,gh}(\omega)$ is the *spectral coherence function* for the signals, which has the property $0 \leq |\gamma_{s,gh}(\omega)| \leq 1$. We will elaborate the interpretation of signal coherence in Section 3, but coherence magnitude < 1 models random effects in the propagation paths from the source to arrays g and h . Note that our assumption of perfect spatial coherence across individual arrays implies that the random propagation effects have negligible impact on the intra-array delays τ_{hn} in (2) and the bearings ϕ_1, \dots, ϕ_H .

The signal received at sensor n on array h is modeled as a sum of the delayed source signal and noise,

$$z_{hn}(t) = s_h(t - \tau_h - \tau_{hn}) + w_{hn}(t), \quad (8)$$

where the noise signals $w_{hn}(t)$ are modeled as real-valued, continuous-time, zero-mean, jointly wide-sense stationary, Gaussian random processes that are mutually uncorrelated at distinct sensors, and are uncorrelated from the signals. That is, the noise correlation properties are

$$E\{w_{gm}(t + \tau)w_{hn}(t)\} = r_w(\tau) \delta_{gh} \delta_{mn} \quad (9)$$

$$E\{w_{gm}(t + \tau)s_h(t)\} = 0, \quad (10)$$

where $r_w(\tau)$ is the noise autocorrelation function, and the noise PSD is $G_w(\omega) = \mathcal{F}\{r_w(\tau)\}$. We then collect the observations at each array h into $N_h \times 1$ vectors $\mathbf{z}_h(t) = [z_{h1}(t), \dots, z_{h,N_h}(t)]^T$ for $h = 1, \dots, H$, and we further collect the observations from the H arrays into a $(N_1 + \dots + N_H) \times 1$ vector

$$\mathbf{Z}(t) = \begin{bmatrix} \mathbf{z}_1(t) \\ \vdots \\ \mathbf{z}_H(t) \end{bmatrix}. \quad (11)$$

The elements of $\mathbf{Z}(t)$ in (11) are zero-mean, jointly wide-sense stationary, Gaussian random processes. We can express the CSD matrix of $\mathbf{Z}(t)$ in a convenient form with the following definitions. The array manifold for array h at frequency ω is

$$\mathbf{a}_h(\omega) = \begin{bmatrix} \exp(-j\omega\tau_{h1}) \\ \vdots \\ \exp(-j\omega\tau_{h,N_h}) \end{bmatrix} = \begin{bmatrix} \exp[j\frac{\omega}{c}((\cos\phi_h)\Delta x_{h1} + (\sin\phi_h)\Delta y_{h1})] \\ \vdots \\ \exp[j\frac{\omega}{c}((\cos\phi_h)\Delta x_{h,N_h} + (\sin\phi_h)\Delta y_{h,N_h})] \end{bmatrix}, \quad (12)$$

using τ_{hn} from (2) and assuming that the sensors have omnidirectional response to sources in the plane of the array. Let us define the relative time delay of the signal at arrays g and h as

$$D_{gh} = \tau_g - \tau_h, \quad (13)$$

where τ_h is defined in (1). Then the cross-spectral density matrix of $\mathbf{Z}(t)$ in (11) has the form

$$\mathbf{G}_Z(\omega) = \begin{bmatrix} \mathbf{a}_1(\omega)\mathbf{a}_1(\omega)^H G_{s,11}(\omega) & \cdots & \mathbf{a}_1(\omega)\mathbf{a}_H(\omega)^H \exp(-j\omega D_{1H})G_{s,1H}(\omega) \\ \vdots & \ddots & \vdots \\ \mathbf{a}_H(\omega)\mathbf{a}_1(\omega)^H \exp(+j\omega D_{1H})G_{s,1H}(\omega)^* & \cdots & \mathbf{a}_H(\omega)\mathbf{a}_H(\omega)^H G_{s,HH}(\omega) \end{bmatrix} + G_w(\omega)\mathbf{I}. \quad (14)$$

The source CSD functions $G_{s,gh}(\omega)$ in (14) can be expressed in terms of the signal spectral coherence $\gamma_{s,gh}(\omega)$ using (7). Note that (14) depends on the source location parameters (x_s, y_s) through the bearings ϕ_h in $\mathbf{a}_h(\omega)$ and the pairwise time-delay differences D_{gh} .

2.1 Cramér-Rao Bound (CRB)

The Cramér-Rao bound (CRB) provides a lower bound on the variance of any unbiased estimator. The problem of interest is estimation of the source location parameter vector $\Theta = [x_s, y_s]^T$ using T samples of the sensor signals $\mathbf{Z}(0), \mathbf{Z}(T_s), \dots, \mathbf{Z}((T-1) \cdot T_s)$, where T_s is the sampling period. The total observation time is $\mathcal{T} = T \cdot T_s$. Let us denote the sampling rate by $f_s = 1/T_s$ and $\omega_s = 2\pi f_s$. We will assume that the continuous-time random processes $\mathbf{Z}(t)$ are band-limited, and that the sampling rate f_s is greater than twice the bandwidth of the processes. Then Friedlander [8, 9] has shown that the Fisher information matrix (FIM) \mathbf{J} for the parameters Θ based on the samples $\mathbf{Z}(0), \mathbf{Z}(T_s), \dots, \mathbf{Z}((T-1) \cdot T_s)$ has elements

$$J_{ij} = \frac{\mathcal{T}}{4\pi} \int_0^{\omega_s} \text{tr} \left\{ \frac{\partial \mathbf{G}_Z(\omega)}{\partial \theta_i} \mathbf{G}_Z(\omega)^{-1} \frac{\partial \mathbf{G}_Z(\omega)}{\partial \theta_j} \mathbf{G}_Z(\omega)^{-1} \right\} d\omega, \quad i, j = 1, 2, \quad (15)$$

where “tr” denotes the trace of the matrix. The CRB matrix $\mathbf{C} = \mathbf{J}^{-1}$ then has the property that the covariance matrix of any unbiased estimator $\hat{\Theta}$ satisfies $\text{Cov}(\hat{\Theta}) - \mathbf{C} \geq \mathbf{0}$, where $\geq \mathbf{0}$ means that $\text{Cov}(\hat{\Theta}) - \mathbf{C}$ is positive semidefinite [10]. Equation (15) provides a convenient way to compute the FIM for the distributed sensor array model as a function of the signal coherence between distributed arrays, the signal and noise bandwidth and power spectra, and the sensor placement geometry. The CRB is evaluated for various scenarios in [6, 7].

3 TIME-DELAY ESTIMATION (TDE)

Let us parameterize the model in (14) by the bearings ϕ_h and the time-delay differences D_{gh} . Then we must address the issue of time-delay estimation with signals that are *partially* coherent when $|\gamma_{s,gh}| < 1$. We consider this problem first for the case of $H = 2$ sensors, as illustrated in Figure 2a with the differential time delay defined as $D = D_{21}$. It follows from (14) that the CSD matrix of the sensor data in Figure 2a is

$$\text{CSD} \begin{bmatrix} z_1(t) \\ z_2(t) \end{bmatrix} = \begin{bmatrix} G_{s,11}(\omega) & e^{+j\omega D} \gamma_{s,12}(\omega) [G_{s,11}(\omega) G_{s,22}(\omega)]^{1/2} \\ e^{-j\omega D} \gamma_{s,12}(\omega)^* [G_{s,11}(\omega) G_{s,22}(\omega)]^{1/2} & G_{s,22}(\omega) \end{bmatrix}. \quad (16)$$

The signal coherence function $\gamma_{s,12}(\omega)$ describes the degree of correlation that remains in the signal emitted by the source at each frequency ω after propagating to sensors 1 and 2. Since the sensor signals are modeled as Gaussian random processes, the coherence loss can be equivalently represented in terms of a “coherent” signal component $s(t)$ and additional additive noise processes $n_1(t), n_2(t)$, as depicted in Figure 2b.¹ The equivalence is

$$\begin{aligned} z_1(t) &= s_1(t) + w_1(t) = (h_1 * s)(t) + n_1(t) + w_1(t) \\ z_2(t) &= s_2(t - D) + w_2(t) = (h_2 * s)(t - D) + n_2(t) + w_2(t), \end{aligned} \quad (17)$$

where $*$ denotes convolution. The parameters in the CSD (16) are related to the filters $H_i(\omega) = \mathcal{F}\{h_i(t)\}$, $i = 1, 2$, the PSDs $G_i(\omega)$, $i = 1, 2$ of the noise processes² $n_i(t)$, $i = 1, 2$ and the PSD $G_c(\omega)$ of $s(t)$ as follows:

$$H_1(\omega) = G_{s,11}(\omega)^{1/2} \quad (18)$$

$$H_2(\omega) = \frac{\gamma_{s,12}(\omega)^*}{|\gamma_{s,12}(\omega)|} G_{s,22}(\omega)^{1/2} \quad (19)$$

$$\text{PSD}[s(t)] = G_c(\omega) = |\gamma_{s,12}(\omega)| \quad (20)$$

$$\text{PSD}[n_1(t)] = G_1(\omega) = G_{s,11}(\omega) [1 - |\gamma_{s,12}(\omega)|] \quad (21)$$

$$\text{PSD}[n_2(t)] = G_2(\omega) = G_{s,22}(\omega) [1 - |\gamma_{s,12}(\omega)|]. \quad (22)$$

Note that we can define a “coherent” signal-to-noise (SNR) ratio at each sensor, based on the coherent signal component in Figure 2b:

$$\text{SNR}_{c,i}(\omega) = \frac{|\gamma_{s,12}(\omega)|}{1 - |\gamma_{s,12}(\omega)| + \left(\frac{G_{s,ii}(\omega)}{G_w(\omega)}\right)^{-1}} \leq \frac{|\gamma_{s,12}(\omega)|}{1 - |\gamma_{s,12}(\omega)|}, \quad i = 1, 2. \quad (23)$$

The coherent SNR is severely limited when there is coherence loss ($|\gamma_{s,12}(\omega)| < 1$) between the sensors, even if the source power is very large ($G_{s,ii}(\omega) \rightarrow \infty$).

¹The equivalent model is developed in [7], and it is also discussed in the context of ultrasound image speckle in [12].

²The processes $n_1(t), n_2(t)$ are independent, zero mean, stationary Gaussian random processes that are independent from the signals and noise $w_1(t), w_2(t)$.

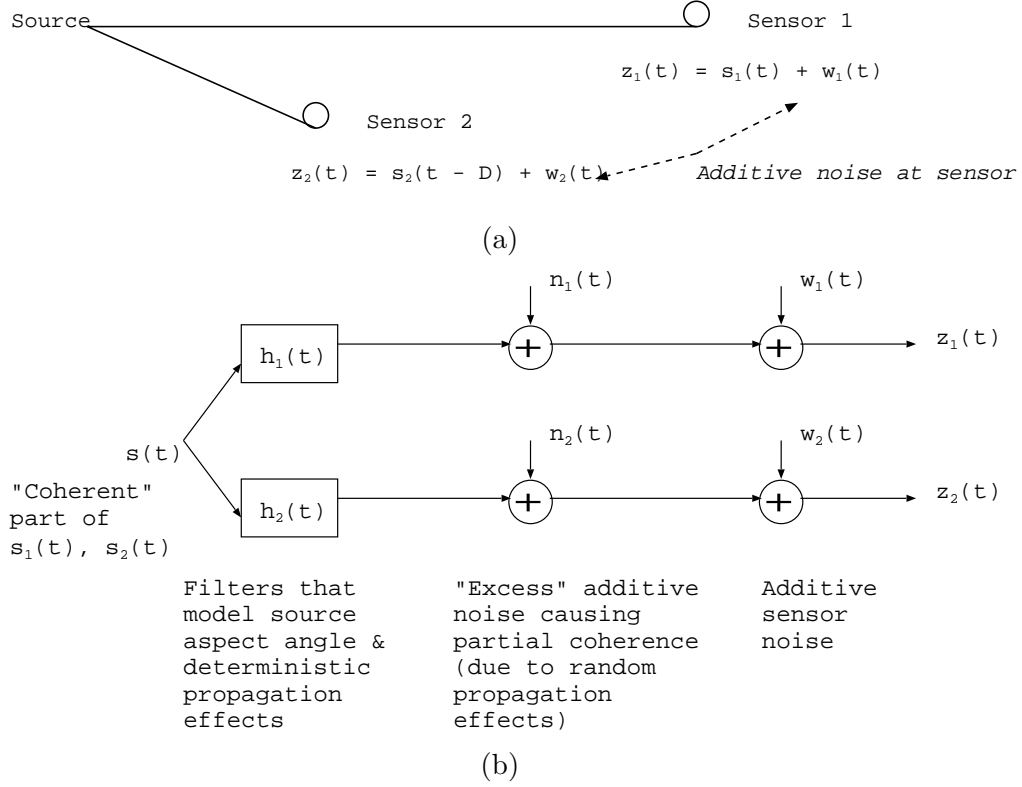


Figure 2: (a) Time-delay estimation (TDE) problem for a non-moving source. (b) Representation of partial coherence between $s_1(t), s_2(t)$ as excess additive noise $n_1(t), n_2(t)$.

3.1 TDE Performance Bounds

In this section, we summarize and further study performance bounds on time-delay estimation (TDE) with partially coherent signals that were originally presented in [6, 7]. First, the CRB on estimating the time-delay D in (16) is, using (15),

$$\text{CRB}(D) = \frac{4\pi}{\mathcal{T}} \left[\int_0^{\omega_s} \frac{\omega^2 |\gamma_{s,12}(\omega)|^2 \frac{G_{s,11}(\omega)G_{s,22}(\omega)}{G_w(\omega)^2}}{1 + \frac{G_{s,11}(\omega)}{G_w(\omega)} + \frac{G_{s,22}(\omega)}{G_w(\omega)} + [1 - |\gamma_{s,12}(\omega)|^2] \frac{G_{s,11}(\omega)G_{s,22}(\omega)}{G_w(\omega)^2}} d\omega \right]^{-1} \quad (24)$$

$$= \frac{4\pi}{\mathcal{T}} \left[\int_0^{\omega_s} \frac{\omega^2 \text{SNR}_{c,1}(\omega) \cdot \text{SNR}_{c,2}(\omega)}{1 + \text{SNR}_{c,1}(\omega) + \text{SNR}_{c,2}(\omega)} d\omega \right]^{-1}, \quad (25)$$

where \mathcal{T} is the total observation time of the sensor data and $\text{SNR}_{c,i}(\omega)$, the coherent SNR, is defined in (23). Let us consider the case in which the signal PSDs, noise PSDs, and coherence are flat (constant) over a frequency band from f_1 to f_2 Hz, and let us define $\text{SNR}_i = G_{s,ii}/G_w$, $i = 1, 2$. Then the CRB in (24) reduces to³

$$\text{CRB}(D) = \frac{3}{8\pi^2 \mathcal{T} (f_2^3 - f_1^3)} \left[\frac{1}{|\gamma_{s,12}|^2} - 1 + \frac{1}{|\gamma_{s,12}|^2} \cdot \frac{1 + \text{SNR}_1 + \text{SNR}_2}{\text{SNR}_1 \text{SNR}_2} \right] \quad (26)$$

$$> \frac{3}{8\pi^2 \mathcal{T} (f_2^3 - f_1^3)} \left[\frac{1}{|\gamma_{s,12}|^2} - 1 \right], \quad (27)$$

³The CRB in (26) can also be derived from results in [11] based on the equivalent model in (18)-(22).

where (27) is the high-SNR limit. Note that partially coherent signals $|\gamma_{s,12}| < 1$ limit the TDE accuracy in a way that cannot be improved by increased source power. Improved TDE accuracy is obtained with partially coherent signals by increased observation time \mathcal{T} or increased signal bandwidth $[f_1, f_2]$. The source signal bandwidth is not controllable in passive source localization applications, so increased observation time is the only means for improving the accuracy of TDE with partially coherent signals. Source motion becomes more important during long observation times, and we add motion into the model in Section 4.

It is well-known that the CRB on TDE is achievable only when the coherent SNR at the two sensors exceeds a threshold [13]. For the case of TDE with partially coherent signals, we showed in [7] that a similar threshold phenomenon occurs with respect to *coherence*. That is, the coherence must exceed a threshold in order to achieve the CRB (24) on TDE. We can state the formula for threshold coherence for the following scenario. The signal and noise spectra are flat over a bandwidth of $\Delta\omega$ rad/sec centered at ω_0 rad/sec, and the observation time is \mathcal{T} seconds. Further, assume that the signal PSDs are identical at each sensor, and define the following constants for notational simplicity:

$$G_{s,11}(\omega_0) = G_{s,22}(\omega_0) = G_s, \quad G_w(\omega_0) = G_w, \quad \gamma_{s,12}(\omega_0) = \gamma_s. \quad (28)$$

Then combining the equivalent model (18)-(22) with previously developed Ziv-Zakai bounds on TDE [13], we can show that the following SNR-like expression characterizes the performance of time delay estimation with partially coherent signals:

$$\text{SNR}(\gamma_s) = \left[\frac{1}{|\gamma_s|^2} \left(1 + \frac{1}{(G_s/G_w)} \right)^2 - 1 \right]^{-1}. \quad (29)$$

The threshold SNR for CRB attainability [13] is a function of the time-bandwidth product $\left(\frac{\Delta\omega \cdot \mathcal{T}}{2\pi}\right)$ and the fractional bandwidth $\left(\frac{\Delta\omega}{\omega_0}\right)$,

$$\text{SNR}_{\text{thresh}} = \frac{6}{\pi^2 \left(\frac{\Delta\omega \mathcal{T}}{2\pi}\right)} \left(\frac{\omega_0}{\Delta\omega}\right)^2 \left[\varphi^{-1} \left(\frac{1}{24} \left(\frac{\Delta\omega}{\omega_0}\right)^2 \right) \right]^2, \quad (30)$$

where $\varphi(y) = 1/\sqrt{2\pi} \int_y^\infty \exp(-t^2/2) dt$. It follows that the threshold coherence value is

$$|\gamma_s|^2 \geq \frac{\left(1 + \frac{1}{(G_s/G_w)}\right)^2}{1 + \frac{1}{\text{SNR}_{\text{thresh}}}}, \quad \text{so} \quad |\gamma_s|^2 \geq \frac{1}{1 + \frac{1}{\text{SNR}_{\text{thresh}}}} \quad \text{as} \quad \frac{G_s}{G_w} \rightarrow \infty. \quad (31)$$

For a specific narrowband time delay estimation scenario, the threshold SNR for CRB attainability is given by (30), and (31) provides a corresponding threshold coherence for CRB attainability. Since $|\gamma_s|^2 \leq 1$, (31) is useful only if $G_s/G_w > \text{SNR}_{\text{thresh}}$.

Figure 3 contains plots of the threshold coherence in (31) as a function of the time-bandwidth product $\left(\frac{\Delta\omega \cdot \mathcal{T}}{2\pi}\right)$, SNR $\frac{G_s}{G_w}$, and fractional bandwidth $\left(\frac{\Delta\omega}{\omega_0}\right)$. Note that $\frac{G_s}{G_w} = 10$ dB is nearly equivalent to $\frac{G_s}{G_w} \rightarrow \infty$. The variation of threshold coherence with fractional bandwidth is illustrated in Figure 3d. We note that very large time-bandwidth product is required to overcome coherence loss when the fractional bandwidth is small at 0.1. For a fixed threshold coherence value, such as 0.7, each doubling of the fractional bandwidth reduces the required time-bandwidth product by about a factor of 10.

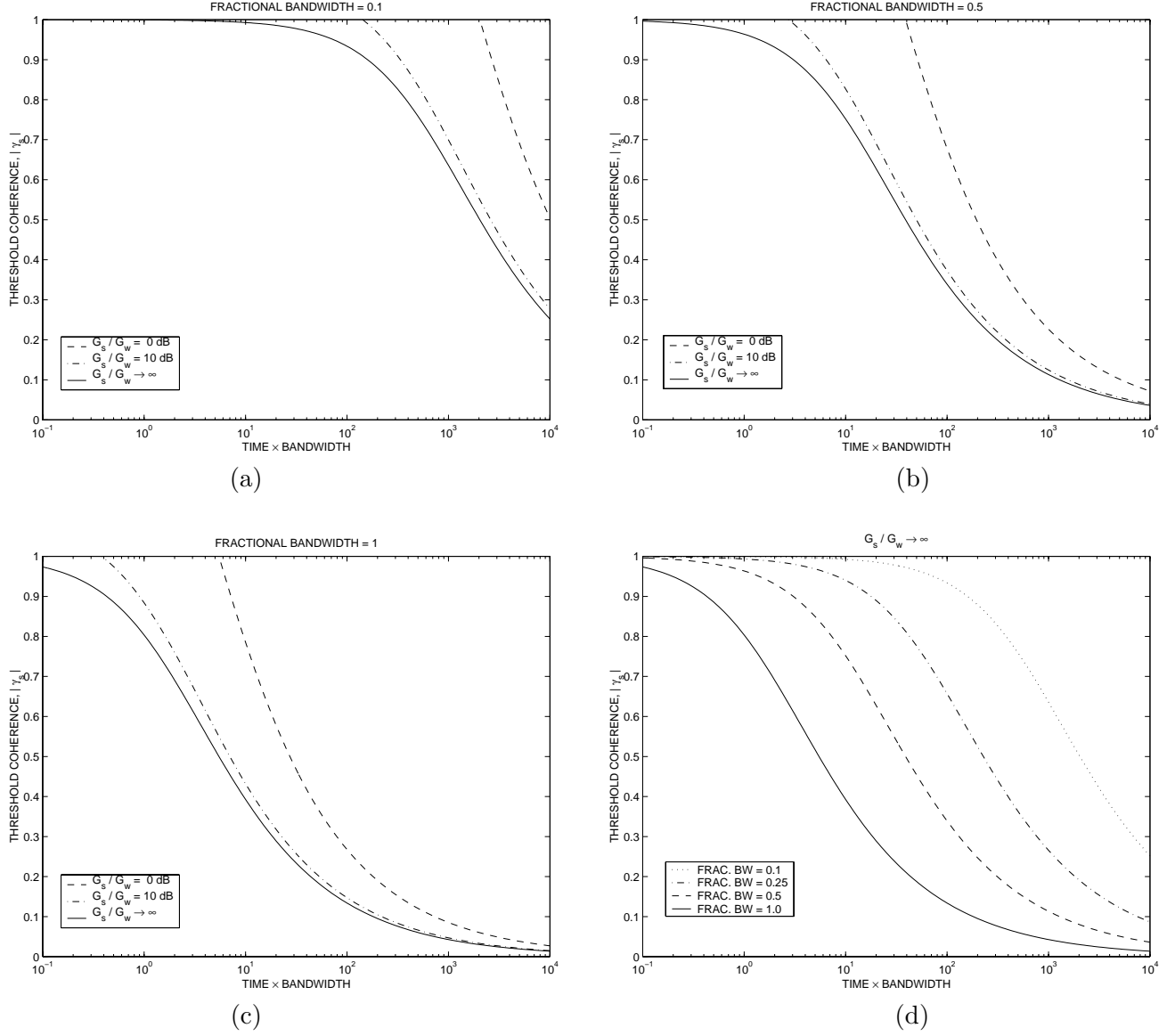


Figure 3: Threshold coherence value from (31) versus time-bandwidth product $\left(\frac{\Delta\omega \cdot T}{2\pi}\right)$ and SNR G_s/G_w for fractional bandwidth values $\left(\frac{\Delta\omega}{\omega_0}\right)$ (a) 0.1, (b) 0.5, (c) 1.0. In (d), the high SNR curves $G_s/G_w \rightarrow \infty$ are superimposed for several values of fractional bandwidth.

Let us examine a narrowband signal scenario that is typical in aeroacoustics, with center frequency $f_o = \omega_o/(2\pi) = 50$ Hz and bandwidth $\Delta f = \Delta\omega/(2\pi) = 5$ Hz, so the fractional bandwidth is $\Delta f/f_o = 0.1$. From Figure 3a, coherence $|\gamma_s| = 0.8$ requires time-bandwidth product $\Delta f \cdot T > 200$, so the necessary time duration $T = 40$ sec for TDE is impractically large for most cases with moving sources.

Increased time-bandwidth product of the observed signals is necessary to make TDE feasible in environments with signal coherence loss. As discussed with respect to the CRB, only the observation time is controllable in passive applications, thus leading us to consider source motion models in Section 4 for use during long observation intervals. The remainder of this section continues to focus on non-moving sources, with simulation results presented in Section 3.2 that verify the CRB and threshold coherence values for TDE, and a discussion in Section 3.3 that extends the $H = 2$ sensor case of this subsection to TDE with $H > 2$ sensors.

3.2 TDE Simulation Examples

Consider TDE at $H = 2$ sensors with varying signal coherence γ_s . Our first simulation example involves a signal with reasonably wide bandwidth, $\Delta f = 30$ Hz centered at $f_0 = 100$ Hz, so the fractional bandwidth $\Delta f/f_0 = 0.3$. The signal, noise, and coherence are flat over the frequency band, with SNR $G_s/G_w = 100$ (20 dB). The signals and noise are band-pass Gaussian random processes. The sampling rate in the simulation is $F_s = 10^4$ samples/sec, with $T = 3 \times 10^4$ samples, so the time interval length is $T = 3$ sec.

Figure 4a displays the simulated RMS error on TDE for $0.2 \leq \gamma_s \leq 1.0$, along with the corresponding CRB from (26). The simulated RMS error is based on 100 runs, and the TDE is estimated from the location of the maximum of the cross-correlation of the sensor signals. The threshold coherence for this case is 0.41, from (31). Note in Figure 4a that the simulated RMS error on TDE diverges sharply from the CRB very near to the threshold coherence value of 0.41, illustrating the accuracy of the analytical threshold coherence in (31).

Next we consider TDE with three different signals:

1. A narrowband signal with $\Delta f = 2$ Hz centered at $f_0 = 40$ Hz. We refer to this as “1 harmonic” (it is the fundamental frequency of the signals defined next).
2. “2 harmonics” at 40 and 80 Hz, with bandwidth $\Delta f = 2$ Hz at each harmonic.
3. “5 harmonics” at 40, 80, 120, 160, 200 Hz, with bandwidth $\Delta f = 2$ Hz at each harmonic.

The signal, noise, and coherence are flat over each frequency band, with SNR $G_s/G_w = 100$ (20 dB), and the signals and noise are band-pass Gaussian random processes. The sampling rate in the simulation is $F_s = 10^4$ samples/sec, with $T = 2 \times 10^4$ samples, so the time interval length is $T = 2$ sec.

Figures 4b-d display the simulated RMS error on TDE (based on 1,000 runs) for coherence values $0.7 \leq \gamma_s \leq 1.0$. As in the previous example, the TDE is obtained by cross-correlation. The threshold coherence is defined only for the “1 harmonic” signal, and the threshold coherence value is ≈ 1 . Figure 4b illustrates the divergence of the simulated RMS error from the CRB, except at $\gamma_s = 1$.

Figures 4c and d display the results for the signals with “2 harmonics” and “5 harmonics.” The additional harmonics enable accurate TDE for lower coherence values, but we cannot use (31) to compute the analytical threshold coherence for the harmonic signals. The “approximate threshold coherence” values indicated in Figures 4c and d are computed as follows. For the K harmonics, suppose the *total bandwidth* of all harmonics, $\Delta f = K \cdot 2$ Hz, is centered at the fundamental

frequency $f_0 = 40$ Hz. The approximate threshold coherence values, 0.95 in Figure 4c and 0.50 in Figure 4d, are considerably lower than the actual points of divergence from the CRB. Not surprisingly, the total bandwidth that is “spread” across the harmonics is less useful for overcoming signal coherence loss than an equivalent bandwidth concentrated at the fundamental $f_0 = 40$ Hz. Narrowband and harmonic signals are generally difficult for TDE due to ambiguous peaks in the cross-correlation function.

3.3 TDE with $H > 2$ Sensors

Weinstein [14] has studied TDE with a network of $H > 2$ sensors. In this section, we extend his analysis to partially coherent signals, and show that *pairwise* TDE is essentially optimum for cases of interest with reasonable signal coherence between sensors. By pairwise TDE we mean that one sensor, say H , is identified as the reference, and only the $H - 1$ time differences $D_{1H}, D_{2H}, \dots, D_{H-1,H}$ are estimated. Under the conditions described below, these $H - 1$ estimates are nearly as accurate for source localization as forming *all pairs* of TDEs D_{gh} for all $g < h$. Weinstein’s analysis [14] is valid for moving as well as non-moving sources.

Assuming equal SNR_c at all sensors, equal coherence γ_s between all sensor pairs, and $H \cdot \text{SNR}_c \gg 1$, we can show that forming all TDE pairs D_{gh} potentially improves the source localization variance relative to pairwise processing by the factor

$$V = \frac{H \left(1 + 2 \cdot \frac{\gamma_s}{1 - \gamma_s} \right)}{2 \left(1 + H \cdot \frac{\gamma_s}{1 - \gamma_s} \right)}. \quad (32)$$

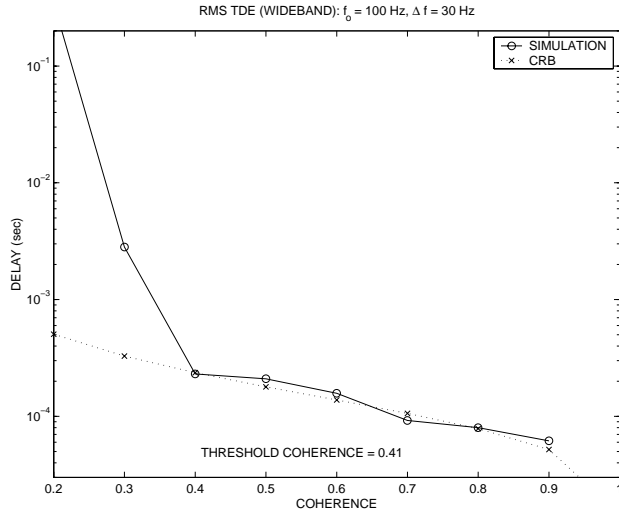
Clearly $V \rightarrow 1$ as $\gamma_s \rightarrow 1$, and $V < (3H)/[2(1 + H)] < 1.5$ for $\gamma_s > 0.5$. Therefore the potential accuracy gain from processing all sensor pairs is negligible when the coherence exceeds the threshold values that are typically required for TDE.

This result suggests strategies with moderate communication bandwidth that potentially achieve nearly optimum localization performance. The reference sensor, H , sends its raw data to all other sensors. Those sensors $h = 1, \dots, H - 1$, locally estimate the time differences $D_{1H}, \dots, D_{H-1,H}$, and these estimates are passed to the fusion center for localization processing with the bearing estimates ϕ_1, \dots, ϕ_H . A modified scheme with more communication bandwidth but more centralized processing is for all H sensors to communicate their data to the fusion center, with TDE performed at the fusion center.

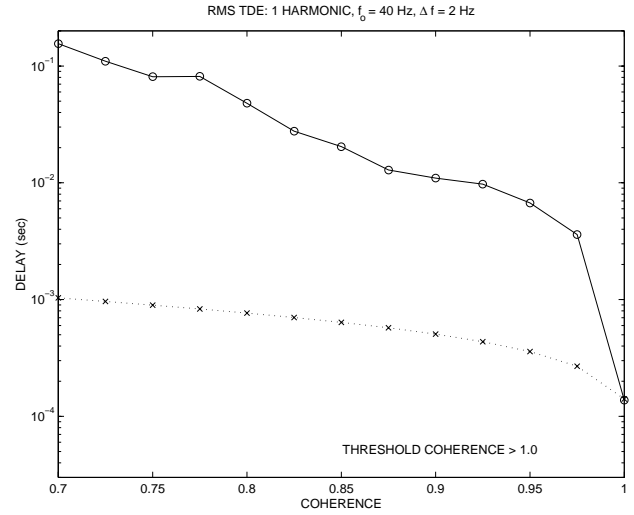
4 DATA MODEL FOR A MOVING SOURCE

Our objective in this paper is to quantify scenarios in which jointly processing data from widely-spaced sensors has the potential for improved source localization accuracy, compared with incoherent triangulation/tracking of bearing estimates. We established in Section 2 that the potential for improved accuracy depends directly on TDE between the sensors. Then we showed in Section 3 that TDE with partially-coherent signals is feasible only with an increased time-bandwidth product of the sensor signals. This leads to a constraint on the minimum observation time, \mathcal{T} , in passive applications where the signal bandwidth is fixed. If the source is moving, then approximating it as non-moving becomes poorer as \mathcal{T} increases, so modeling the source motion becomes more important.

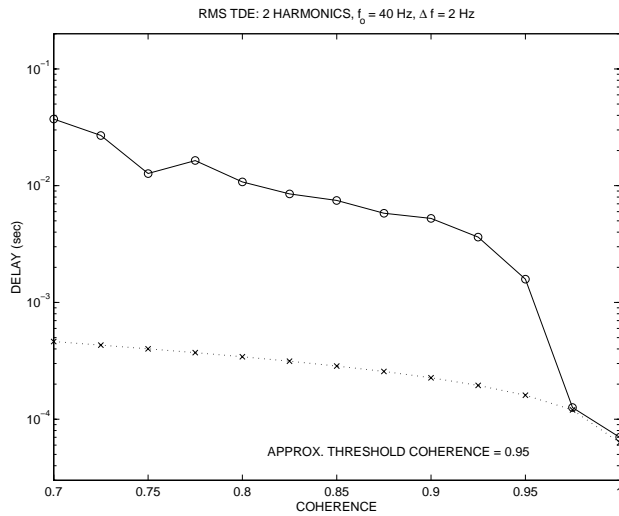
Approximate bounds are developed in [15] and [16] that specify conditions of validity for non-moving and moving source models. Let us consider $H = 2$ sensors with Doppler values $\alpha_2 > \alpha_1$ (see



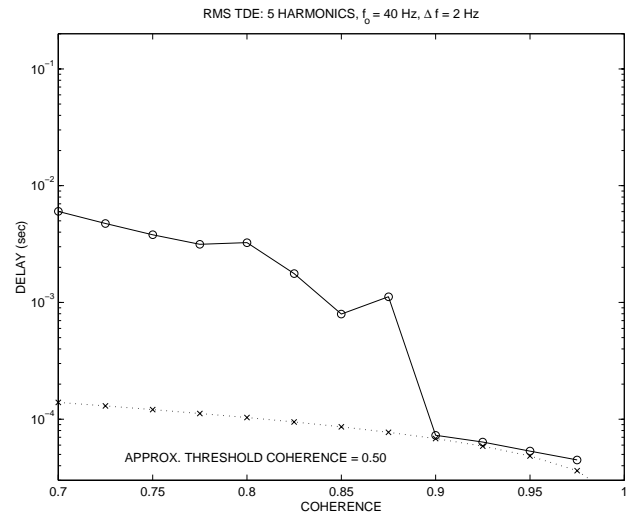
(a)



(b)



(c)



(d)

Figure 4: Comparison of simulated RMS error for TDE with CRBs and threshold coherence value. (a) Wideband signal with $\Delta f = 30$ Hz centered at $f_0 = 100$ Hz. (b)-(d) Narrowband signal with $\Delta f = 2$ Hz, fundamental frequency $f_0 = 40$ Hz and 1, 2, and 5 harmonic components, respectively.

(46) for the definitions of α_1, α_2). If f_{\max} (Hz) is the maximum signal frequency that is processed, then TDE estimation accuracy is not seriously affected by ignoring source motion, as long as the time interval \mathcal{T} satisfies

$$\mathcal{T} \ll \frac{1}{f_{\max} \left(\frac{\alpha_2}{\alpha_1} - 1 \right)}. \quad (33)$$

Taking typical parameters for ground vehicles in aeroacoustics, let us consider a vehicle moving at 5% the speed of sound (15 m/sec), with radial motion that is in opposite directions at the two sensors. Then $\alpha_2/\alpha_1 - 1 \approx 0.1$ and (33) becomes $\mathcal{T} \ll 10/f_{\max}$. For $f_{\max} = 100$ Hz, the requirement is $\mathcal{T} \ll 0.1$ sec, which according to the analysis in Section 3.1 yields insufficient time-bandwidth product for partially coherent signals that are typically encountered. Thus motion modeling and Doppler compensation are critical, even for aeroacoustic sources that move more slowly than in this example.

In this section, we extend the non-moving source model from Section 2 using first-order motion models (see (34),(35),(49)). The first-order motion models are simple and accurate over larger time intervals \mathcal{T} compared with the non-moving source model. However, accurate modeling of more complex trajectories over longer time intervals requires higher-order polynomial models, with added complexity. The source position trajectory is modeled as a straight line with constant velocity over an interval of length \mathcal{T} ,

$$x_s(t) = x_{s,0} + \dot{x}_s \cdot (t - t_0), \quad t_0 \leq t \leq t_0 + \mathcal{T} \quad (34)$$

$$y_s(t) = y_{s,0} + \dot{y}_s \cdot (t - t_0), \quad (35)$$

so \dot{x}_s, \dot{y}_s are the velocity components. The source trajectory parameter vector is

$$\Theta = [x_{s,0}, \dot{x}_s, y_{s,0}, \dot{y}_s]^T, \quad (36)$$

and the (time-varying) propagation time from the source to the sensors on array h follows from (1) and (2):

$$\tau_h(t) = \frac{d_h(t)}{c} = \frac{1}{c} \left[(x_s(t) - x_h)^2 + (y_s(t) - y_h)^2 \right]^{1/2} \quad (37)$$

$$\begin{aligned} \tau_{hn}(t) &\approx -\frac{1}{c} \left[\frac{x_s(t) - x_h}{d_h(t)} \Delta x_{hn} + \frac{y_s(t) - y_h}{d_h(t)} \Delta y_{hn} \right] \\ &= -\frac{1}{c} [(\cos \phi_h(t)) \Delta x_{hn} + (\sin \phi_h(t)) \Delta y_{hn}]. \end{aligned} \quad (38)$$

The bearing and bearing rate are related to the source motion parameters Θ as

$$\phi_h(t) = \tan^{-1} \left[\frac{x_s(t) - x_h}{y_s(t) - y_h} \right] = \tan^{-1} \left[\frac{x_{s,0} + \dot{x}_s \cdot (t - t_0) - x_h}{y_{s,0} + \dot{y}_s \cdot (t - t_0) - y_h} \right] \quad (39)$$

$$\dot{\phi}_h(t) = \frac{\dot{y}_s \cos \phi_h(t) - \dot{x}_s \sin \phi_h(t)}{d_h(t)}. \quad (40)$$

The radial velocity of the source with respect to array h is

$$v_{r,h}(t) = \dot{x}_s \cos \phi_h(t) + \dot{y}_s \sin \phi_h(t). \quad (41)$$

We can insert (34) and (35) into (37) to obtain the following approximation for the propagation time to array h :

$$\tau_h(t) = \tau_h(t_0) \left[1 + \frac{2 \cdot \cos \phi_h(t_0) \cdot \dot{x}_s \cdot (t - t_0)}{d_h(t_0)} + \frac{2 \cdot \sin \phi_h(t_0) \cdot \dot{y}_s \cdot (t - t_0)}{d_h(t_0)} \right]^{1/2} \quad (42)$$

$$\approx \tau_h(t_0) + \frac{v_{r,h}(t_0)}{c} \cdot (t - t_0), \quad (43)$$

where $d_h(t_0)$ and $v_{r,h}(t_0)$ are the source distance and radial velocity at the start of time interval $t = t_0$. The approximation (43) is valid as long as the total motion during the time interval \mathcal{T} is much less than the range, i.e., $|2\dot{x}_s\mathcal{T}| \ll d_h(t_0)$ and $|2\dot{y}_s\mathcal{T}| \ll d_h(t_0)$.

Next we use the approximation (43) and model the received signal at the reference sensor on array h as

$$s_h(t - \tau_h(t)) = s_h \left[\left(1 - \frac{v_{r,h}(t_0)}{c} \right) t - \tau_h(t_0) + \frac{v_{r,h}(t_0)t_0}{c} \right] \quad (44)$$

$$= s_h \left(\alpha_h t - \tau_h(t_0) + \frac{v_{r,h}(t_0)t_0}{c} \right), \quad t_0 \leq t \leq t_0 + \mathcal{T}, \quad (45)$$

where

$$\alpha_h = 1 - \frac{v_{r,h}(t_0)}{c} = 1 - \frac{1}{c} [\dot{x}_s \cos \phi_h(t_0) + \dot{y}_s \sin \phi_h(t_0)] \quad (46)$$

is the Doppler compression and

$$\tau_h(t_0) = \frac{d_h(t_0)}{c} = \frac{1}{c} [(x_{s,0} - x_h)^2 + (y_{s,0} - y_h)^2]^{1/2} \quad (47)$$

is the propagation delay at the initial time $t = t_0$. Without loss of generality, we set $t_0 = 0$, so the received signal at sensor n on array h is

$$s_h(\alpha_h t - \tau_h(0) - \tau_{hn}(t)), \quad (48)$$

which is the extension of the signal component of (8) to the moving source case. Note from (2) that $\tau_{hn}(t)$ depends on the source location only through the time-varying bearing $\phi_h(t)$, which we approximate with a first-order model

$$\phi_h(t) \approx \phi_h(t_0) + \dot{\phi}(t_0) \cdot (t - t_0), \quad t_0 \leq t \leq t_0 + \mathcal{T}. \quad (49)$$

For a single array h , the Doppler compression α_h and time delay $\tau_h(t_0)$ have negligible effect on estimation of the intra-array delays $\tau_{hn}(t)$, since α_h and $\tau_h(t_0)$ are identical for each $n = 1, \dots, N_h$. Thus each array can be processed separately to estimate the bearings $\phi_1(t_0), \dots, \phi_H(t_0)$ and bearing rates $\dot{\phi}_1(t_0), \dots, \dot{\phi}_H(t_0)$, and these can be “triangulated” via (39) and (40) to estimate the source motion parameters Θ in (36). An algorithm [17] for estimating $\phi_h(t_0)$ and $\dot{\phi}_h(t_0)$ is described in Section 5 and demonstrated with measured data in Section 6.

Let us consider the signals received at the reference sensors at each array, so $\tau_{hn}(t) = 0$ in (48):

$$s_1 \left[\left(1 - \frac{v_{r,1}(t_0)}{c} \right) t - \tau_1(t_0) \right], \dots, s_H \left[\left(1 - \frac{v_{r,H}(t_0)}{c} \right) t - \tau_H(t_0) \right]. \quad (50)$$

Our modeling assumptions imply that each signal $s_h \left[\left(1 - \frac{v_{r,h}(t_0)}{c} \right) t - \tau_h(t_0) \right]$ is a wide-sense stationary Gaussian random process. However, for two arrays g, h with *unequal* Doppler $v_{r,g}(t_0) \neq v_{r,h}(t_0)$, the signals at arrays g, h are *not* jointly wide-sense stationary [15, 18], complicating the analytical description and the CRB performance analysis. The jointly nonstationary sensor signals generally are not characterized by a cross-spectral density matrix, so the CRB is not the inverse of a FIM of the form (15). An approximate CRB analysis for TDE with jointly nonstationary signals as in (50) is given in [15]. The CRB analysis is rigorously justified in [18] and extended to CRBs on differential Doppler. A clever transformation is used in [18] so that the jointly nonstationary signals in (50) are locally modeled by a CSD of the form (14), and it is shown that the representation is accurate for CRB analysis.

We can formulate the results in [18] for the case of partially coherent signals⁴, leading to the following for $H = 2$ arrays, assuming large time-bandwidth product (much larger than the coherence time of the signals and noise). We define the TDE $D_{12} = \tau_1(t_0) - \tau_2(t_0)$ and the differential Doppler $\Delta v_{12} = v_{r,1}(t_0) - v_{r,2}(t_0)$.

- Estimation of TDE and differential Doppler are decoupled, so the CRB on D_{12} is given by (25), which is identical to the non-moving source case.
- The threshold coherence analysis for TDE in (31) and Figure 3 extends to the moving source case. In the best case that Doppler effects are perfectly estimated and compensated, the TDE problem that remains is identical to the non-moving source case. Doppler estimation is less demanding in terms of time-bandwidth product compared with TDE. Indeed, Doppler estimation is possible with sinusoidal signals [18] that have negligible bandwidth.
- The CRB on differential Doppler [18], modified for partially-coherent signals and assuming $\text{SNR}_{c,1}(\omega) = \text{SNR}_{c,2}(\omega) = \text{SNR}_c(\omega)$, is

$$\text{CRB}(\Delta v_{12}) = \frac{24\pi}{\mathcal{T}} \left(\frac{c}{\mathcal{T}} \right)^2 \left[2 \int_0^{\omega_s} \frac{\omega^2 \text{SNR}_c(\omega)^2}{1 + 2 \cdot \text{SNR}_c(\omega)} d\omega \right]^{-1}. \quad (51)$$

Note that (51) is a scalar multiple of the CRB on TDE in (25). However, the CRB on differential Doppler may be achievable in scenarios in which the time-bandwidth product is insufficient for TDE.

Interestingly, differential Doppler provides sufficient information for source localization, even without TDE, as long as five or more sensors are available [18]. Thus the source motion may be exploited in scenarios where TDE is not feasible, such as narrowband signals [18].

- We discussed TDE with $H > 2$ sensors in Section 3.3, concluding that pairwise processing of TDEs $D_{1H}, \dots, D_{H-1,H}$ with a reference sensor H is nearly optimum for scenarios of interest. A similar result holds for differential Doppler estimation [18], where pairwise estimation of $\Delta v_{1H}, \dots, \Delta v_{H-1,H}$ is nearly as accurate as estimation of all pairs Δv_{gh} , as long as $H \cdot \text{SNR}_c(\omega) \gg 1$.

5 AN ALGORITHM

The parameters that can be directly estimated from the sensor data are the bearings $\phi_1(t_0), \dots, \phi_H(t_0)$, bearing rates $\dot{\phi}_1(t_0), \dots, \dot{\phi}_H(t_0)$, pairwise time differences $D_{1H} = \tau_1(t_0) - \tau_H(t_0)$, \dots , $D_{H-1,H} = \tau_{H-1}(t_0) - \tau_H(t_0)$, and differential Doppler $\Delta v_{1H} = v_{r,1}(t_0) - v_{r,H}(t_0)$, \dots , $\Delta v_{H-1,H} = v_{r,H-1}(t_0) - v_{r,H}(t_0)$. Equations (39), (40), (46), (47) define the nonlinear relations that “triangulate” these parameters and relate them to the source motion parameters $\Theta = [x_{s,0}, \dot{x}_s, y_{s,0}, \dot{y}_s]^T$.

A distributed processing algorithm is outlined below, and parts of the algorithm are illustrated with measured aeroacoustic data in the next section.

1. Use the local polynomial approximation (LPA) beamformer [17] at each array to estimate the bearings and bearing rates. The LPA beamformer in [17] is formulated for narrowband processing, and it is a generalization of the classical beamformer to moving sources. We extend it in a straightforward way to wideband signals by incoherently averaging the LPA beampatterns at different frequencies.

⁴The signal coherence between the signals at arrays g and h in (50) is defined assuming perfect compensation of the Doppler compression α_g, α_h , thus yielding the definition in (7).

2. Solve (39), (40) to obtain initial estimates of the source motion parameters Θ . These estimates correspond to incoherent triangulation of the bearings and bearing rates from individual arrays.
3. Estimate the Doppler compression factors $\alpha_1, \dots, \alpha_H$, compensate for Doppler, and test whether the signals at distinct arrays have sufficient coherence, fractional bandwidth, and time-bandwidth product to enable TDE between arrays (see Section 3.1 for the conditions).
4. If the conditions are *not* met, then incoherent triangulation of the bearings and bearing rates is nearly optimum, and further joint processing is not informative.
5. If the conditions are met, then identify a reference array H (the array with maximum SNR) and estimate the time differences $D_{1H}, \dots, D_{H-1,H}$ and differential Dopplers $\Delta v_{1H}, \dots, \Delta v_{H-1,H}$. Many estimation methods have been studied for this problem, e.g., [19]-[27]. The maximum likelihood solution involves wideband ambiguity function search over Doppler and TDE [15], while the deskewed short-time correlator [22] is a computationally simpler approximation.
6. A suboptimum procedure is to avoid the joint Doppler and TDE estimation in the preceding step, and instead use the *initial* Doppler estimates from steps 1 and 2 and perform TDE after approximate Doppler compensation. With this approach, triangulation of the TDEs via (47) will improve the estimates of $x_{s,0}$ and $y_{s,0}$ only (and not the source velocity \dot{x}_s, \dot{y}_s).
7. If multiple sources are present, then the LPA beamformer in step 1 may be used to separate the source signals at each array prior to Doppler/TDE estimation. We note that wideband beamforming algorithms for non-moving source models are presented in [28, 29] and [30]-[32].

The LPA beamformer in steps 1 and 7 is illustrated in the next section for a two-source scenario based on measured aeroacoustic data. Examples of TDE with Doppler compensation (step 5) are presented in [33].

6 EXAMPLE WITH TWO MOVING SOURCES

We present an application of the local polynomial approximation (LPA) beamformer [17] to measured aeroacoustic data with two ground vehicles: M1 and M3 tanks. The vehicle trajectories over a 10 second segment are shown in Figure 5a. Two arrays, labeled 8B and 8C, are separated by about 23 m. Each array is circular with $N = 7$ sensors, 4-ft radius, and six sensors equally spaced around the perimeter with one sensor in the center. We present results based on processing the data at array 8B, for which the bearing and bearing rate of the sources are shown in Figure 5b. The bearing of the M3 varies by more than 30° over the 10 second time interval. The range of the M3 is closer at about 100 m, with the M1 range at approximately 200 m.

The data from array 8B is processed over a wide bandwidth from 30 to 150 Hz. The beampattern for a classical beamformer based on a non-moving source model is shown in Figure 5c. The beampattern is the incoherent sum of narrowband beampatterns over the 30 to 150 Hz frequency band. The peak of the beampattern is located at approximately the mean bearing of the stronger source (M3) over the 10 second interval.

The beampattern of the LPA beamformer is shown in Figure 6a. The LPA beampattern exploits a first-order model for time-varying bearing, as in (49). The LPA beampattern is two-dimensional, with axes of initial bearing $\phi(t_0)$ and bearing rate $\dot{\phi}(t_0)$. The LPA beamformer in [17] is

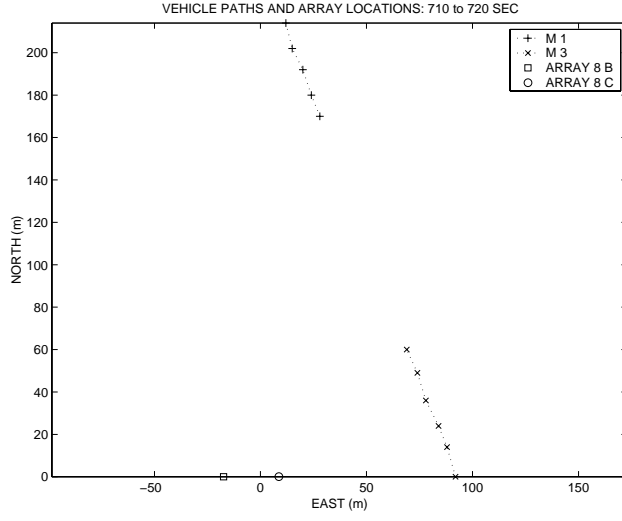
formulated for narrowband processing, so we extend to the wideband case by incoherently adding the narrowband LPA beampatterns over the frequency range. The peak of the beampattern in Figure 6a is close to the true values of $\phi(t_0)$, $\dot{\phi}(t_0)$ for the M3 that are shown in Figure 5b. The location of the weaker M1 source is not evident in the LPA beampattern in Figure 6a, so we subtract an estimate of the stronger source from the data. The subtraction is performed based on the bearing and bearing rate estimates from Figure 6a. The subtraction is coherent over the processing bandwidth and includes the time-varying bearing. The LPA beampattern after subtraction is shown in Figure 6b, which indicates the bearing and bearing rate of the weaker M1 source. This example illustrates the gain in resolution that is achieved by exploiting the source motion in a beamformer.

7 CONCLUDING REMARKS

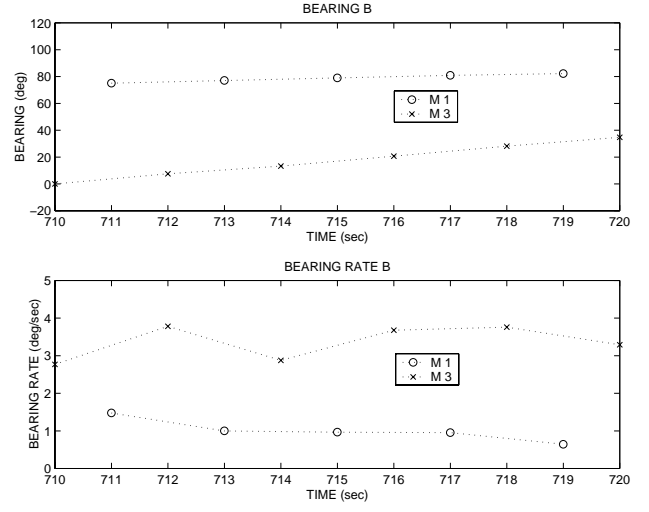
The potential gain in source localization accuracy when data from distributed arrays is processed jointly and coherently is quantified by the CRBs presented in this paper. The amount of improvement and the feasibility of achieving the improvement depend critically on the scenario, which is characterized by the coherence between source signals arriving at distributed sensors, the signal bandwidth and spectrum shape (wideband vs. harmonic), the observation time for coherent processing, the noise level, the source motion parameters (velocity, complexity of maneuvers), and the number of sources. In feasible scenarios in which the time-bandwidth product is large enough to enable TDE, we presented an algorithm that requires moderate communication bandwidth between sensors. The processing involves estimation of bearing and bearing rate at individual arrays, and estimation of time delay and differential Doppler between pairs of arrays.

References

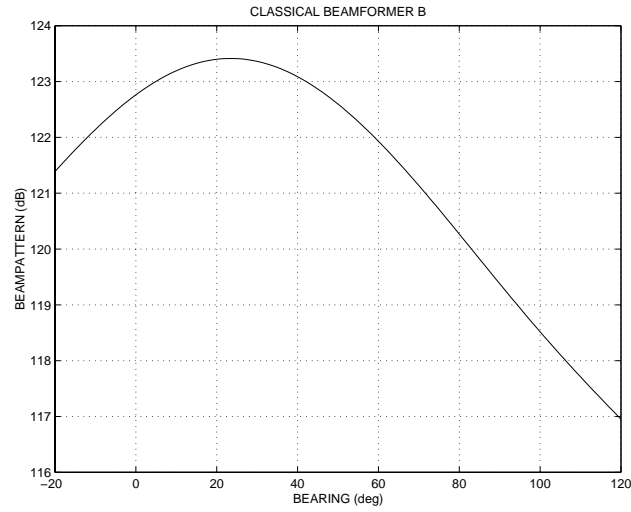
- [1] R.R. Tenney and J.R. Delaney, "A distributed aeroacoustic tracking algorithm," *Proc. American Control Conf.*, pp. 1440-1450, June 1984.
- [2] Y. Bar-Shalom and X.-R. Li, *Multitarget-Multisensor Tracking: Principles and Techniques*, YBS, 1995.
- [3] A. Farina, "Target tracking with bearings-only measurements," *Signal Processing*, vol. 78, pp. 61-78, 1999.
- [4] B. Ristic, S. Arulampalam, C. Musso, "The influence of communication bandwidth on target tracking with angle only measurements from two platforms," *Signal Processing*, vol. 81, pp. 1801-1811, 2001.
- [5] L.M. Kaplan, P. Molnar, Q. Le, "Bearings-only target localization for an acoustical unattended ground sensor network," *Proc. SPIE AeroSense*, Orlando, Florida, April 2001.
- [6] R.J. Kozick and B.M. Sadler, "Distributed Sensor Array Processing of Wideband Acoustic Signals," 1999 Meeting of the IRIS Specialty Group on Battlefield Acoustics and Seismics, Laurel, MD, September 13-15, 1999.
- [7] R.J. Kozick and B.M. Sadler, "Algorithms for Localization and Tracking of Acoustic Sources with Widely Separated Sensors," *Proc. 2000 Meeting of the MSS Specialty Group on Battlefield Acoustics and Seismics*, Laurel, MD, October 18-20, 2000.
- [8] B. Friedlander, "On the Cramer-Rao Bound for Time Delay and Doppler Estimation," *IEEE Trans. on Info. Theory*, vol. IT-30, no. 3, pp. 575-580, May 1984.



(a)



(b)



(c)

Figure 5: (a) Array locations and trajectory of M1 and M3 vehicles over a 10 second time interval. (b) Bearing and bearing rate of sources with respect to array 8 B. (c) Beampattern of classical beamformer based on non-moving source model.

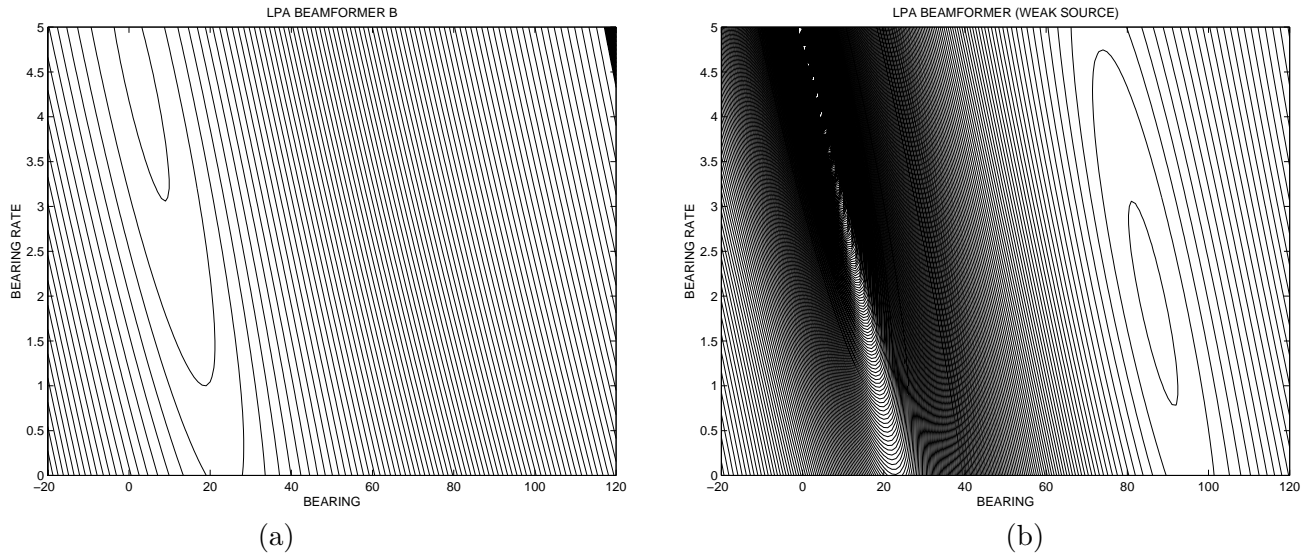


Figure 6: (a) Beampattern of LPA beamformer, showing the location of the stronger source (M3). (b) Beampattern of LPA beamformer after subtracting an estimate of the strong source signal from the data, showing the location of the weaker source (M1).

- [9] P. Whittle, "The analysis of multiple stationary time series," *J. Royal Statist. Soc.*, vol. 15, pp. 125-139, 1953.
- [10] S.M. Kay, *Fundamentals of Statistical Signal Processing: Estimation Theory*, Prentice-Hall, 1993.
- [11] G.C. Carter (ed.), *Coherence and Time Delay Estimation* (Selected Reprint Volume), IEEE Press, 1993.
- [12] I. Cespedes, J. Ophir, S.K. Alam, "The combined effect of signal decorrelation and random noise on the variance of time delay estimation," *IEEE Trans. on Ultrasonics, Ferroelectrics, and Frequency Control*, vol. 44, no. 1, pp. 220-225, Jan. 1997.
- [13] A.J. Weiss and E. Weinstein, "Fundamental limitations in passive time delay estimation - part 1: narrowband systems," *IEEE Trans. Acoust., Speech, Sig. Proc.*, vol. ASSP-31, no. 2, pp. 472-485, April 1983.
- [14] E. Weinstein, "Decentralization of the Gaussian maximum likelihood estimator and its applications to passive array processing," *IEEE Trans. Acoust., Speech, Sig. Proc.*, vol. ASSP-29, no. 5, pp. 945-951, October 1981.
- [15] C.H. Knapp and G.C. Carter, "Estimation of time delay in the presence of source or receiver motion," *J. Acoust. Soc. Am.*, vol. 61, no. 6, pp. 1545-1549, June 1977.
- [16] W.B. Adams, J.P. Kuhn, W.P. Whyland, "Correlator compensation requirements for passive time-delay estimation with moving source or receivers," *IEEE Trans. Acoust., Speech, Signal Processing*, vol. ASSP-28, no. 2, pp. 158-168, April 1980.
- [17] V. Katkovnik and A.B. Gershman, "A local polynomial approximation based beamforming for source localization and tracking in nonstationary environments," *IEEE Signal Processing Letters*, vol. 7, no. 1, pp. 3-5, Jan. 2000.
- [18] P.M. Schultheiss and E. Weinstein, "Estimation of differential Doppler shifts," *J. Acoust. Soc. Am.*, vol. 66, no. 5, pp. 1412-1419, Nov. 1979.

- [19] B.V. Hamon and E.J. Hannon, "Spectral estimation of time delay for dispersive and non-dispersive systems," *Applied Statistics*, vol. 23, issue 2, pp. 134-142, 1974.
- [20] J.A. Stuller, "Maximum-likelihood estimation of time-varying delay - part I," *IEEE Trans. Acoust., Speech, Signal Processing*, vol. ASSP-35, no. 3, pp. 300-313, March 1987.
- [21] J.A. Stuller and N. Hubing, "New perspectives for maximum likelihood time-delay estimation," *IEEE Trans. on Signal Processing*, vol. 45, no. 3, pp. 513-525, March 1997.
- [22] J.W. Betz, "Comparison of the deskewed short-time correlator and the maximum likelihood correlator," *IEEE Trans. Acoust., Speech, Signal Processing*, vol. ASSP-32, no. 2, pp. 285-294, April 1984.
- [23] L.G. Weiss, "Wavelets and wideband correlation processing," *IEEE Signal Processing Magazine*, pp. 13-32, Jan. 1994.
- [24] M. Wax, "The joint estimation of differential delay, Doppler, and phase," *IEEE Trans. on Information Theory*, vol. IT-28, no. 5, pp. 817-820, Sept. 1982.
- [25] S. Stein, "Differential delay/Doppler ML estimation with unknown signals," *IEEE Trans. on Signal Processing*, vol. 41, no. 8, pp. 2717-2719, Aug. 1993.
- [26] Q. Jin, K.M. Wong, Z.-Q. Luo, "The estimation of time delay and Doppler stretch of wideband signals," *IEEE Trans. on Signal Processing*, vol. 43, no. 4, pp. 904-916, April 1995.
- [27] R.J. Ulman and E. Geraniotis, "Wideband TDOA/FDOA processing using summation of short-time CAF's," *IEEE Trans. on Signal Processing*, vol. 47, no. 12, pp. 3193-3200, Dec. 1999.
- [28] K. Bell, "Separation of multiple battlefield acoustic targets using wideband DF-based adaptive beam-forming," 1999 Meeting of the IRIS Specialty Group on Battlefield Acoustics and Seismics, Laurel, MD, September 13-15, 1999.
- [29] K. Bell, "Wideband direction-of-arrival (DOA) estimation for multiple aeroacoustic sources," Proc. 2000 Meeting of the MSS Specialty Group on Battlefield Acoustics and Seismics, Laurel, MD, October 18-20, 2000.
- [30] T. Pham and B. M. Sadler, "Adaptive wideband aeroacoustic array processing," *8th IEEE Statistical Signal and Array Processing Workshop*, pp. 295-298, Corfu, Greece, June 1996.
- [31] T. Pham and B. Sadler, "Incoherent and coherent wideband direction finding algorithms for ground vehicles," *132nd Meeting of the Acoustic Society of America, JASA* vol. 100, no. 4, pt. 2, p. 2636, October 1996.
- [32] T. Pham and B. M. Sadler, "Focused wideband array processing algorithms for high-resolution direction finding," *IRIS Battlefield Acoustics Symposium*, October 1998.
- [33] R.J. Kozick and B.M. Sadler, "Near-Field Localization of Acoustic Sources with Imperfect Spatial Coherence, Distributed Processing, and Low Communication Bandwidth," *SPIE 2001 AeroSense Symp.*, Orlando, FL, April, 2001.